Materials Characterization 145 (2018) 644–652

Contents lists available at ScienceDirect

Materials Characterization

journal homepage: www.elsevier.com/locate/matchar

Mechanical properties of Al/ω-Al-Cu-Fe composites synthesized by the SPS technique

Aurélie Joseph[a], Véronique Gauthier-Brunet[a], Anne Joulain[a,*], Joël Bonneville[a], Sylvain Dubois[a], Jean-Philippe Monchoux[b], Frédéric Pailloux[a]

[a] Institut Pprime, CNRS, Université de Poitiers, ISAE-ENSMA, UPR 3346, BP 30179, 86962, Futuroscope, Chasseneuil Cedex, France
[b] Centre d'Elaboration de Matériaux et d'Etudes Structurales (CEMES), CNRS UPR 8011, BP 94347, 31055 Toulouse Cedex 4, France

ARTICLE INFO

Keywords:
Metal matrix composite
Al-Cu-Fe alloy
Phase transformation
Mechanical properties
Microstructure
Spark plasma sintering

ABSTRACT

Al/40 vol%ω-Al-Cu-Fe composites were produced from Al powder and i-Al-Cu-Fe quasi-crystalline particles using spark plasma sintering (SPS) technique. The mechanical properties of the composite were evaluated over the temperature range 293 K–823 K by performing compression tests at constant strain rate. The temperature dependence of the $\sigma_{0,2\%}$ yield stress gives evidence of two temperature regimes with a transition in the range 473 K–523 K. The decrease of $\sigma_{0,2\%}$ with increasing temperature, more pronounced in the low temperature regime, indicates that the two temperature regimes correspond to two different thermally activated deformation mechanisms. Based on microstructural analyses of the Al matrix, where plastic deformation takes place, the different strengthening contributions are discussed and the results are finally compared to those obtained for composites produced by hot isostatic pressing (HIP), for which the $\sigma_{0,2\%}$ temperature dependence is similar. In the low temperature regime, the $\sigma_{0.2\%}$ stress of the SPS composites is higher than that of the HIP composites. In this temperature regime, the stress difference is mainly ascribed to the different reinforcement phases present in the Al matrix. In the high temperature regime, the temperature dependence of $\sigma_{0.2\%}$ is comparable for the two composites whatever the processing route: load transfer is thus the main strengthening mechanism, which is similar for the two Al/ω-Al-Cu-Fe composites, the temperature dependence being ascribed to cross slip and climb processes.

1. Introduction

Al-based particle-reinforced metal matrix composites (MMC) have a high potential for technological applications, in particular in transport industry, because they meet the criterion of weight reduction and exhibit mechanical properties that cannot be achieved by any Al-based alloy [1–5]. Two categories of particle-reinforced composites must be distinguished. A first category, *in-situ* composites, where reinforcement is formed in the matrix by chemical reactions during the composite fabrication process; the main advantage being a homogeneous distribution of fine particle in the matrix [6–8]. A second category, where particle reinforcement is obtained by embedding hard particles in a metallic matrix. In this case, powder metallurgy processes are mainly employed, which allow an accurate control of particle content and size and the use of a large variety of reinforcement particles.

In the frame of this second category, quasicrystalline (QC) particles present mechanical properties (high hardness together with high elastic modulus and yield stress) and tribological properties that make them promising candidates as reinforcement particles in MMC. Tsaï et al. [9] were the first to fabricate by powder metallurgy route, an Al-based composite reinforced by icosahedral (i) Al-Cu-Fe quasicrystalline particles. Since then, numerous studies have been dedicated to Al/QC composites using different QC alloy systems. Most of them have been devoted to Al-Cu-Fe reinforcement particles [10–24] and to a less extend to Al-Pd-Mn [22,25], Al-Mn-Ce [25], Al-Cr-Mn-Co-Zr [26] and Al-Fe-Cr [27] reinforcement particles. The main reasons for using Al-Cu-Fe QC particles are that the mechanical properties of this QC phase have been well characterized [28–30], they are easy to produce by conventional casting and milling, the alloying elements ensure a low cost production for industrial applications.

Tsaï et al. [9] have shown that, for an Al matrix, a phase transformation takes place during powder metallurgy processing: when the temperature (T_p) is 873 K, the initial QC $Al_{63.5}Cu_{24.0}Fe_{12.5}$ phase transforms into the crystalline ω-$Al_7Cu_2Fe_{10}$ phase [Bown and Brown

* Corresponding author at: CNRS, Université de Poitiers, ENSMA, UPR 3346, SP2MI, Téléport 2 Boulevard Marie et Pierre Curie, BP 30179, F86962, Futuroscope,Chasseneuil Cedex, France.
E-mail address: anne.joulain@univ-poitiers.fr (A. Joulain).

https://doi.org/10.1016/j.matchar.2018.09.025
Received 31 May 2018; Received in revised form 19 July 2018; Accepted 17 September 2018
Available online 18 September 2018
1044-5803/

1956]. For similar composite produced at $T_p = 673$ K, the phase transformation does not occur and the QC phase is preserved. Concerning the mechanical properties, Kaloshkin et al. [18] reported that the yield stress of Al/Al-Cu-Fe composites measured at room temperature was processing temperature dependent. Laplanche et al. [17] compared the mechanical properties of Al/QC-Al-Cu-Fe ($T_p = 673$ K) and Al/ω-Al-Cu-Fe ($T_p = 823$ K) [15] composites, both produced by hot isostatic pressing (HIP) from Al and QC-Al-Cu-Fe powders. By performing compression tests over the temperature range 293 K–823 K, they showed that, below 573 K, the Al/ω-Al-Cu-Fe composites present higher yield stresses than that of the Al/QC-Al-Cu-Fe composites, while they are similar for higher deformation temperatures. Laplanche et al. [31] have also shown that ω-Al-Cu-Fe single-phase and QC-Al-Cu-Fe alloys exhibit similar normalised yield stress in a large temperature range (*i.e.* taking into account of the differences in their elastic coefficients and peritectic temperatures). Therefore, the differences observed between the two composites cannot be ascribed to differences in the mechanical properties of the ω-Al-Cu-Fe and the QC-Al-Cu-Fe phases. In addition, load transfer should be also very similar for both composites, since comparable particles and identical particle volume fraction and size are involved. Thus, the different observed mechanical properties in the temperature range 293 K–573 K may be due to indirect strengthening, that is to different Al-matrix microstructures: the Al-matrix obtained after the phase transformation from QC-$Al_{63.5}Cu_{24.0}Fe_{12.5}$ to ω-$Al_{70}Cu_{20}Fe_{10}$ leading to a more efficient strengthening of the composites.

Most of the studies have used HIP processes. In the present study, the Al/ω-Al-Cu-Fe composites were produced by the SPS (Spark Plasma Sintering) technique, which allows short-time production of large pieces, more suited for industrial applications. Mechanical properties are evaluated by compression test performed at different temperatures. Al-matrix evolutions are analyzed by post-mortem transmission electron microscopy (TEM) observations, that were complemented by *in-situ* heating TEM experiments. The different strengthening contributions are discussed and the results are finally compared to those obtained for composites produced by HIP.

2. Material and Methods

2.1. Synthesis

The production of i-Al-Cu-Fe quasicrystalline material has already been detailed elsewhere [32]. EDS analyses coupled with SEM observations indicate that the i-Al-Cu-Fe phase is predominant and give also evidence of minor phases corresponding to λ-$Al_{13}Fe_4$ and β-$Al_{50}Cu_{50-x}Fe_x$ phases, in good agreement with XRD results [15,33]. The i-$Al_{59\pm2}Cu_{27\pm2}Fe_{13\pm1}$ and commercial Al powders (Alfa Aesar, 99.8 at.% purity, 45–420 μm particle sizes) were used to synthesize the Al/ω-Al-Cu-Fe composites. For this, the i-Al-Cu-Fe powder was obtained by milling a i-Al-Cu-Fe ingot using a planetary ball mill with stainless steel balls and dies. The ball to powder mass ratio is 11 and the rotation speed is 100 rpm. No surfactant was used. Then, i-$Al_{59\pm2}Cu_{27\pm2}Fe_{13\pm1}$ and Al powders were sifted to obtain a particles size smaller than 25 μm and 60 μm, respectively.

To produce Al/40 vol% ω-Al-Cu-Fe composite, Al and 30% vol% of i-Al-Cu-Fe powders [15] were mixed in a Turbula for 30 min. The mixing step allows for the homogenization of the powder distribution. The powder mixtures were then inserted in a graphite die and placed in the Spark Plasma Sintering (SPS) device. They were reactively sintered at $T = 823$ K and a uniaxial pressure P = 100 MPa for 2 min. Commercial Al samples were also densified by SPS using similar parameters. The SPS process has been fully described in [34].

2.2. Microstructural Characterization

The crystallographic structure of the composite material was investigated by X-Ray diffraction (XRD) using a Bruker D8 diffractometer with Cu-$K_{\alpha1}$ radiation. Phase identification was complemented by scanning electron microscopy (SEM) observations using a field-emission gun scanning electron microscope (FESEM, Jeol 7001F-TTLS). The composition was quantified using an energy-dispersive X-ray spectrometer (EDS, Oxford Intruments) with the AZtec software based on PhiRoz correction method. SEM observations were performed using a back-scattered electron (BSE) detector to distinguish the different phase contrasts. The acceleration voltage of the electron beam was set to 15 kV.

The density of the composites has been calculated by accurately measuring the volume and the weight of the cylinder-shape sample.

The local microstructures of the deformed samples were characterized by transmission electron microscopy (TEM) using a Philips CM-20 operating at 200 kV. Slices, with a thickness of about 300 μm, were cut from the bulk sample. They were then pre-thinned up to a thickness of approximately 20 μm by mechanical polishing and glued onto a molybdenum grid. Finally, ion thinning down to electron transparency was performed by means of a Precision Ion Polishing System (Gatan-PIPS). Viguier and Mortensen [35] have shown the effect of the Ar-beam current on precipitate formation due to an excessive sample heating during the preparation of aluminum alloy thin foil. In fact, during ion polishing with an accelerating voltage of 5 kV, an increase of the sample temperature up to 513 K was observed. To reduce this artefact, an operating voltage of 3 kV was first applied followed by a final thinning step at 2.5 kV.

In situ heating treatment was performed on an Al/ω-Al-Cu-Fe composite thin foil using a JEOL-2200FS TEM equipped with a field emission gun (Schottky-FEG) operated at 200 kV and fitted with an in-column Ω-filter. Series of images of the Al/ω-Al-Cu-Fe composite thin foil, using a Gatan Single-Tilt heating holder model 628Ta, were recorded with a Gatan Ultrascan *2 k × 2 k CCD* camera. The absolute temperature of the sample was measured by a thermocouple with an estimated accuracy of ± 10 K. The final temperature, 573 K, was selected by consideration of the mechanical test results. During the heating treatment, the number and size evolutions of precipitates in the Al matrix were monitored. The same area was selected and analyzed at 573 K after 2 min and 1 h20 dwelling times.

2.3. Mechanical Tests

Compression tests were performed using a compression device (Instron 1195), similar to the one described in [36]. Compression samples, whose dimensions are 2.5 × 2.5 × 6 mm^3, were cut with a wire saw. Samples were deformed at a constant strain rate ($\dot{\varepsilon} = 1.4 \times 10^{-4}\,s^{-1}$) at different temperatures ranging between room temperature and 823 K. In order to achieve the thermomechanical stability of the compression set up, when the desired deformation temperature is reached, the sample is then maintained at this temperature for 2 h at least, before starting the compression test. The $\sigma_{0.2\%}$ stress defined at 0.2% plastic strain on the stress-strain curves is used as the characteristic stress for plastic flow. Note that the change in sample cross-section during plastic deformation is taken into account assuming a constant sample volume, so that true stresses and true strains are considered.

3. Results

3.1. Microstructure of As-produced Composites

Representative examples of XRD pattern and SEM micrograph obtained for Al/Al-Cu-Fe composites are shown in Fig. 1a and b, respectively. All diffraction peaks are indexed according to the Al face-centered cubic structure and the ω-Al-Cu-Fe tetragonal structure (Fig. 1a). Based on SEM observations, the Al-Cu-Fe reinforcement particles (grey contrast) are homogeneously distributed into the Al matrix (dark

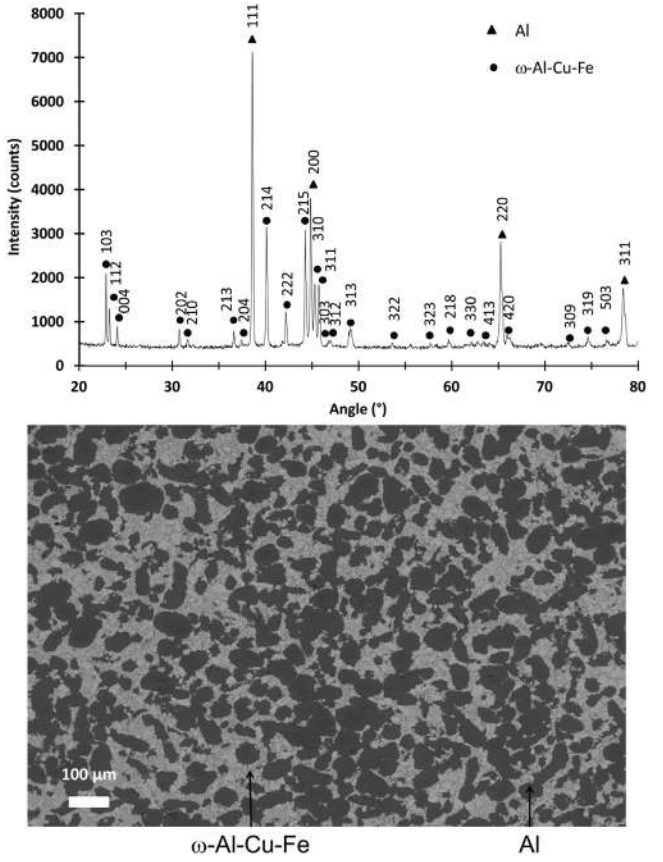

Fig. 1. (a) Typical XRD pattern of the Al/ω-Al-Cu-Fe composite and (b) back-scattered electron (BSE) image of the Al/ω-Al-Cu-Fe composite after reactive SPS sintering at 823 K/100 MPa/2 min.

contrast) (Fig. 1b). From EDS chemical analyses, the chemical compositions of the matrix and the reinforcement particles are $Al_{97 \pm 3}Cu_{2 \pm 2}Fe_{1 \pm 1}$ and $Al_{69 \pm 1}Cu_{20 \pm 2}Fe_{11 \pm 1}$, respectively. Here, the ± sign includes both the measurement errors and the local changes in chemical composition. This result confirms the complete i-Al-Cu-Fe to ω-Al_7Cu_2Fe phase transformation, which is consistent with XRD analyses (Fig. 1a). Image analyses performed with the ImageJ software show a surface fraction of nearly 40% for the reinforcement particles, in agreement with the synthesis of an Al/30% i-Al-Cu-Fe initial composite [3]. The relative density of the composites is close to 99%.

EDS analyses were performed along the dotted line in the Al matrix between two Al/ω particles (see Fig. 2a). Fig. 2b shows the Cu content along this line from point 1 to point 2. The Cu content is highest near the reinforcement particles, with a maximum of about 4 at.% at point 1, and it decreases to 0.5 at.% nearly halfway between the particles. A very low content of Fe (≤0.2 at.%) has only been detected for the three first EDS points close to point 1. The small amount of Fe could be attributed either to the intersection of the electron interaction volume with the Al/ω interface or limited Fe diffusion in the Al matrix. This confirms that we actually measure the Cu content inside the Al grain and not an artefact arising from a potential ω-Al-Cu-Fe reinforcement particle lying below the sample surface, since in such a case a higher Fe content would be detected.

3.2. Mechanical Properties

Fig. 3a shows typical stress-strain curves obtained for Al/ω-Al-Cu-Fe samples deformed at different temperatures. Each sample was deformed up to the fracture. From 293 K to 573 K, the stress-strain curves exhibit a similar behaviour: after an elastic stage, an upper yield stress (UYS) is

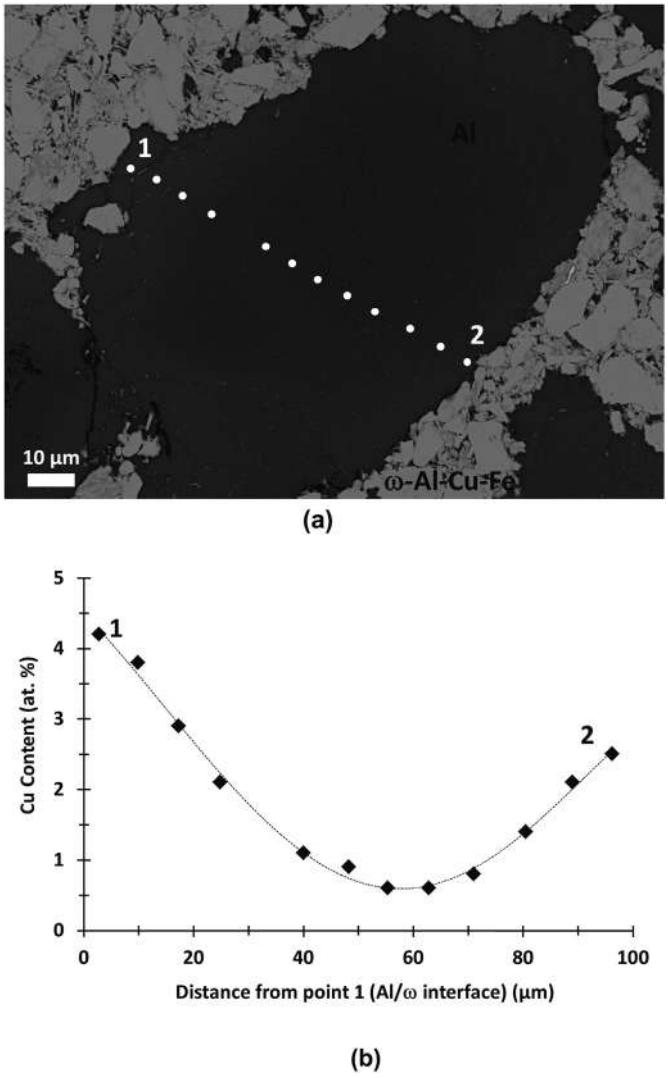

Fig. 2. (a) High magnification BSE image of the Al matrix showing the positions of the EDS analyses (b) Cu content along the dotted line in (a) in the Al matrix.

reached at a plastic deformation of nearly 1% beyond which strain softening takes place only. The UYS, associated with crack initiation, is followed by a fast stress decrease caused by crack propagation, up to complete sample fracture. In the case of the sample deformed at 723 K, the UYS is less pronounced and plastic strain is characterized by a stage of nearly constant hardening.

Fig. 3b presents the change of the $\sigma_{0,2\%}$ stress as a function of temperature for Al/ω-Al-Cu-Fe composite. The $\sigma_{0,2\%}$ stress decreases with increasing temperature, meanwhile the ductility has an opposite behaviour. The continuous decrease of $\sigma_{0,2\%}$ with increasing temperature highlights the role of thermal activation in the deformation mechanisms. A transition temperature, corresponding to a $\sigma_{0,2\%}$ drop of nearly 140 MPa, is observed in the temperature range 473 K–523 K. Below and above the transition temperature, trend lines are drawn on the $\sigma_{0,2\%}$ stress curve. It should be noted that the used linear trend is indicative only and does not necessarily represent the actual temperature dependence of $\sigma_{0,2\%}$.

3.3. Microstructures of Deformed Composites

The Al matrix microstructure of the Al/ω-Al-Cu-Fe composite deformed at room temperature was observed by TEM (Fig. 4a and b). These two micrographs were obtained in the bright-field observation

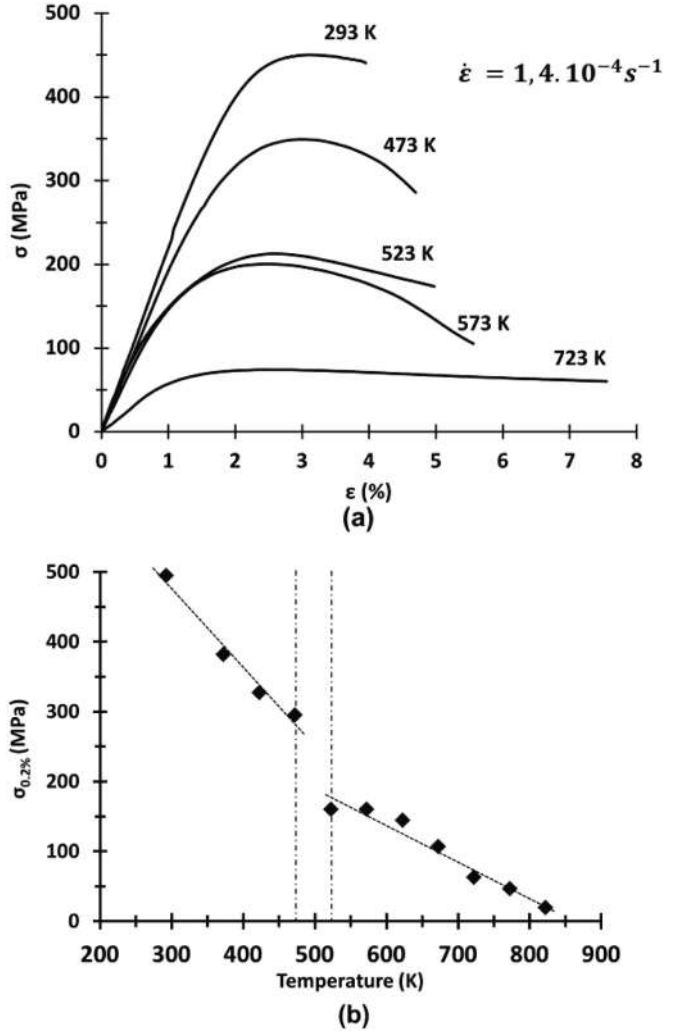

Fig. 3. (a) Stress-strain curves obtained for compression tests performed at different temperatures for Al/ω-Al-Cu-Fe composites. (b) $\sigma_{0,2\%}$ stress as a function of temperature for Al/ω-Al-Cu-Fe composites synthesized by SPS.

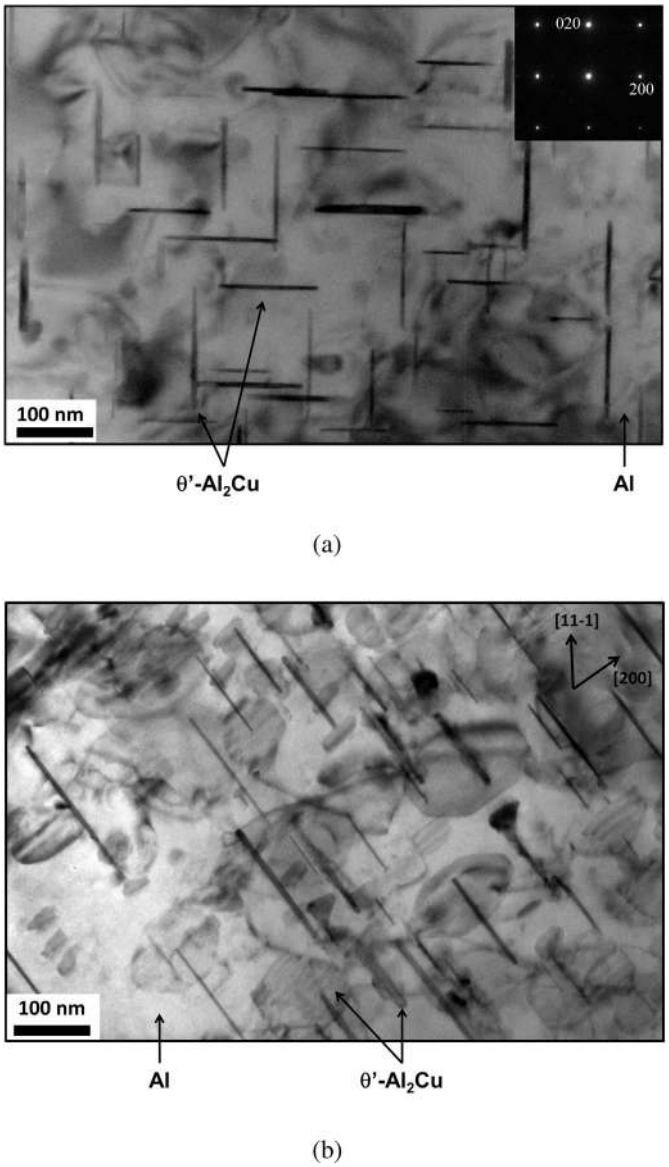

Fig. 4. Al/ω-Al-Cu-Fe composite deformed at 293 K. Bright field TEM images highlighting the presence of θ′-Al_2Cu precipitates in the Al matrix, aligned on (a) [001] zone axis and (b) [011] zone axis. (c) Dark field TEM image in the Al matrix showing the presence of dislocation loops around θ′-Al_2Cu precipitates. The latter are not visible in such diffraction conditions. Smaller loops are also present in the Al matrix.

mode. In Fig. 4a, the Al matrix is aligned along the [001] zone axis, while Fig. 4b is obtained for a [011] zone axis. Fig. 4a exhibits two plate-shaped families observed edge-on and oriented perpendicular to the $[010]_{Al}$ and $[100]_{Al}$ directions of the Al matrix. Note that diffused dark contrast observed in the background (Fig. 4a) is due to variations in local stress level that give rise to dynamical diffracting conditions [37]. A third family perpendicular to the $[001]_{Al}$ can be distinguished, as well. In Fig. 4b, only the family perpendicular to $[100]_{Al}$ is observed edge-on, the two others being inclined within the thin foil. This type of orientation evidences the octagonal shape of the precipitates. The length and the thickness of the precipitates are lower than 200 nm and 25 nm, respectively. All these characteristics (dimension, orientation, shape) strongly suggest that these precipitates correspond to θ′-Al_2Cu [38].

An example of a weak-beam dark field micrograph, obtained in the Al matrix for an Al/ω-Al-Cu-Fe composite deformed at room temperature using the $g = (0\bar{2}2)$ diffraction vector condition, is shown in Fig. 4c. The θ′-Al_2Cu precipitates, not visible with the used diffraction condition, are however revealed by surrounding dislocation loops. Smaller loops, indicated by white arrows in Fig. 4c, are also observed in the Al matrix.

TEM observations were also performed after deformation at 723 K. Fig. 5a shows a bright field TEM image obtained in the Al matrix. The TEM micrograph highlights the presence of plate-shaped θ′-Al_2Cu precipitates. These precipitates present the same shape and the same orientation, with respect to the Al matrix, than those previously observed for the composite deformed at 293 K. According to the precipitate size distribution analyses, the temperature increase involves a coarsening of the precipitates: length and thickness are now lower than 800 nm and 35 nm respectively (200 nm and 25 nm before heating). Moreover, other precipitates (indicated with dashed arrows) with orientations different from the θ' ones are also observed. An example of dark field TEM image performed in the Al matrix is shown in Fig. 5b, using the $g = (2\bar{2}0)$ diffraction vector condition. According to the diffraction conditions, the precipitates are not visible. A high density of dislocations is observed and no dislocation loop surrounding the precipitates is visible.

3.4. In Situ Heating Tests

TEM observations indicate a coarsening of the θ′-Al_2Cu precipitates

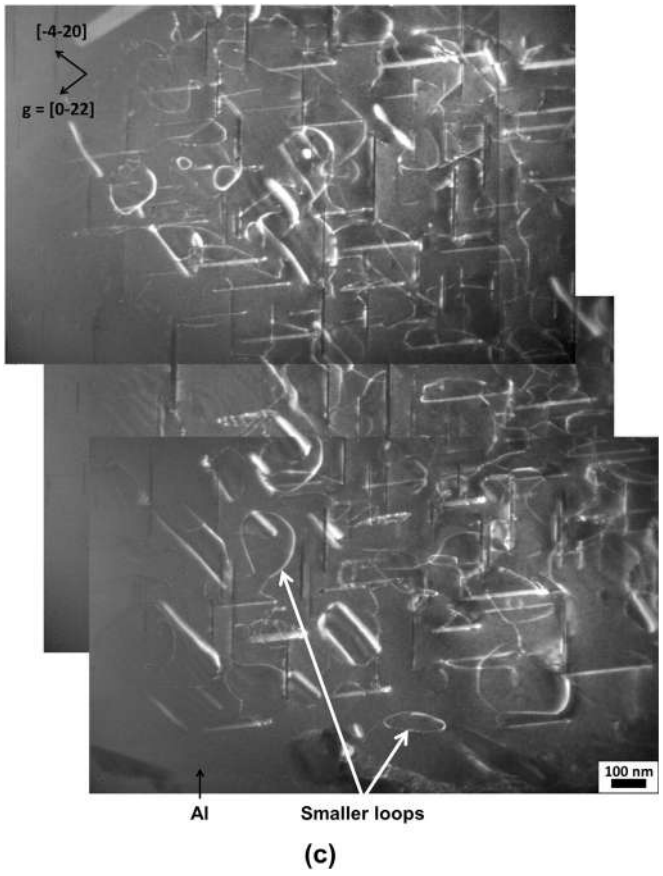

Fig. 4. (*continued*)

in the Al matrix after deformation at 723 K. In order to estimate the microstructural change of the precipitates, *in-situ* heating tests were performed on an Al/ω-Al-Cu-Fe thin foil.

Fig. 6a shows the temperature cycle applied during the heat treatment. Several temperature steps (373 K/23 min and 473 K/4 min) were carried out up to 573 K to observe eventual microstructural changes during heating. The final temperature (573 K) was selected to observe a possible microstructure evolution above the transition temperature (see Fig. 3b). At 573 K, the total observation time was 80 min.

At 373 K and 473 K, no significant change of the microstructure was observed during the observation times of 23 min and 4 min, respectively. At 573 K, after an initial waiting time of 2 min, TEM images were recorded every 3 min. At this temperature, significant changes were observed in both the number and the size of θ′-Al_2Cu precipitates.

To estimate the change in the precipitates characteristics at 573 K, a typical region delimited by a square in Fig. 6b and c was selected on a TEM image. In this area, precipitate characteristics (number, size) were analyzed and compared after 2 min and 80 min. The θ′-Al_2Cu precipitates were divided into two categories (Table 1) depending on their orientation in the thin foil, *i.e.* "edge-on" (refer to as category 1) or "inclined" (refer to as category 2).

After 2 min, the fraction number of precipitates is about 1/3 for the category 1 and 2/3 for the category 2. This result is consistent considering three precipitate families parallel to the three $\{100\}_{Al}$ plane families with two of them belonging to the second category. After 80 min, a drop of approximately 20% in the number of precipitates was observed. The decrease of precipitate number differs according to their category: the decrease is of 32% and of 14% for the first and the second category, respectively. It must be noticed that the decrease differences may also be influenced by thin foil effect, but the overall trend observed after 80 min at this temperature is considered as characteristic of the bulk material.

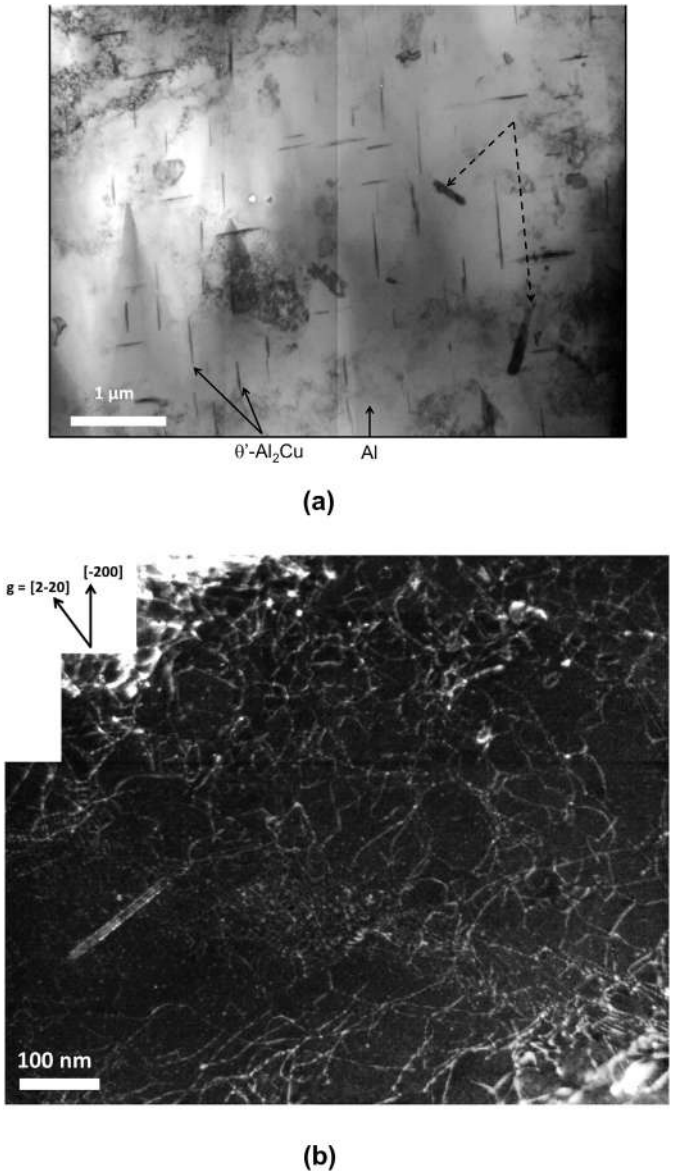

Fig. 5. Al/ω-Al-Cu-Fe composite deformed at 723 K. (a) Bright field TEM images highlighting the presence of θ′-Al_2Cu precipitates (and other precipitates) in the Al matrix. (b) Dark field TEM image in the Al matrix showing the presence of dislocations.

To study the evolution of the θ′-Al_2Cu precipitate size, their length and their thickness measured on Fig. 6b and c were compared (see Table 2). Within this area, the length of a population of 63 precipitates was measured. The thickness measurements, only possible for the category 1 precipitates, were performed on 41 of the 63 selected precipitates previously mentioned. The measurement accuracy is estimated at ± 5 nm. The sizes are reported in. The results show an increase of both the length and the thickness during the *in-situ* heating at 573 K.

4. Discussion

4.1. Relationship Between Microstructure and Mechanical Properties of SPS Composites

It is well established that improvements in the mechanical properties of metal matrix composites result from direct and indirect reinforcements [1,4]. The direct strengthening (also called load transfer) effect occurs when the applied load is transferred from the matrix to the

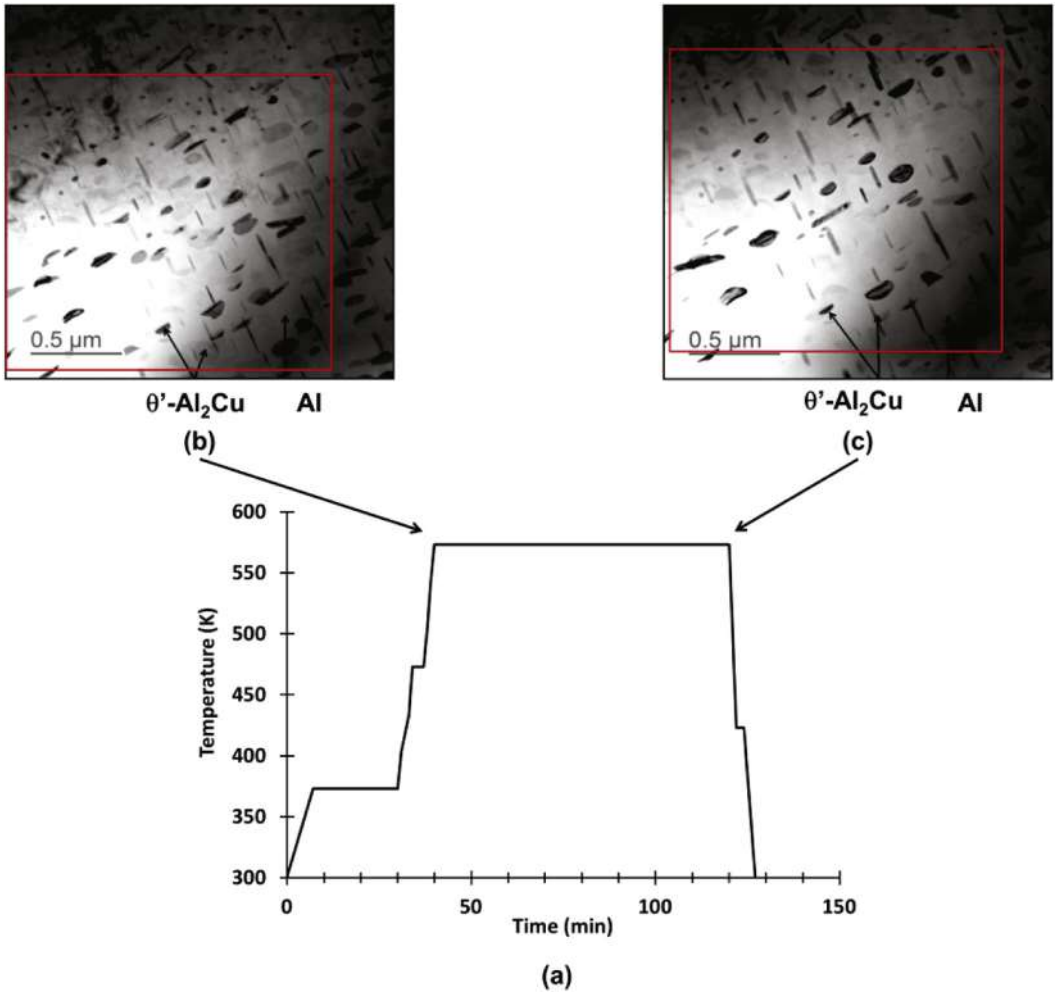

Fig. 6. (a) Temperature cycle performed during the *in situ* thermal treatment in the TEM. Bright field TEM images, obtained during *in-situ* heating at 573 K, showing the θ′-Al_2Cu precipitates in the Al matrix for a holding time of (b) 2 min and (c) 80 min.

Table 1
Number of precipitates for the two categories after 2 min and 80 min at 573 K.

	Number of precipitates		
	Total	Category 1	Category 2
t = 2 min	212	79	133
t = 80 min	168	54	114

Table 2
Dimensions of the precipitates after 2 min and 80 min at 573 K. All sizes are given in nm.

	Mean thickness	Thickness range	Mean length	Length range
t = 2 min	17	7–32	115	32–228
t = 80 min	26	13–44	132	32–284

reinforcement particles. The indirect strengthening is generated by microstructural and composition changes of the matrix consecutive to the interaction with the reinforcement particles during the fabrication process. In the present case, direct strengthening is due to the 40%vol. fraction of the ω reinforcement particles. The presence of Cu in the Al matrix has been revealed by chemical analyses indicating that Cu atoms diffuse into the Al matrix during the composite synthesis. From TEM observations, θ′-Al_2Cu precipitates have also been observed in the Al matrix after deformation at room temperature and at 723 K. Al_2Cu precipitates in a solid solution of Al(Cu) were also observed by Litynska-Dobrzynska et al. [20] in aluminum matrix composites reinforced by quasicrystalline particles. That is here, indirect strengthening is expected to be due to two sources: Al(Cu) solid solution strengthening and Al_2Cu precipitate strengthening.

In previous works dealing with the plastic behaviour of the ω-Al-Cu-Fe phase, Laplanche et al. [16,39] have studied the stress-strain curves of the ω-Al-Cu-Fe phase at different temperatures. They have established the existence of a brittle-to-ductile transition between 700 K and 750 K. At 740 K, the ω-Al-Cu-Fe phase behaves elastically up to approximately 700 MPa. As a consequence, we may reasonably assume that, for the temperatures and stresses used in the present study for the composites, the ω-Al-Cu-Fe phase deforms elastically only and that plastic deformation of the composite is confined in the Al matrix.

Comparison between post-mortem TEM observations performed on the Al/ω-Al-Cu-Fe composites deformed at room temperature and at 723 K shows a change of the dimensions of θ′-Al_2Cu precipitates, the precipitates being larger after deformation at 723 K. These observations are consistent with *in situ* heating tests performed in the TEM. In fact, by comparing the matrix microstructure after 2 min and 80 min at 573 K, a coarsening of the precipitates is observed during thermal treatment: the size of precipitates increases whereas their number decreases. Several studies have been dedicated to the evolution of θ′-Al_2Cu precipitates during isothermal ageing treatments ranging from 383 K to 513 K in the case of Al-4 wt% Cu alloys [40–44]. Boyd and Nicholson [40] have shown that the coarsening rate of the θ′-Al_2Cu precipitates is strongly

temperature dependent. Da Costa Teixeira et al. [44] have studied the effect of the θ′-Al_2Cu precipitates on the strengthening response of Al-3Cu-0.05Sn alloys. From isothermal ageing treatment at 473 K, they have shown that the length and the thickness of the θ′-Al_2Cu precipitates continuously increase whereas the precipitate number remains constant up to about 4 h of ageing time and decreases thereafter. Our results obtained by *in-situ* TEM experiments show similar trends, but at 573 K the number of precipitates already decreases for an ageing time shorter than 80 min. Therefore, our experimental procedure that consists of maintaining the compression samples at the test temperature during at least 2 h prior to deformation is sufficient to induce coarsening of the θ′-Al_2Cu precipitates for temperatures equal to or higher than 573 K.

The temperature dependence of the $\sigma_{0.2\%}$ stress, deduced from the compression tests performed on the Al/ω-Al-Cu-Fe composite, exhibits two temperature regimes with a transition temperature between 473 K and 523 K. The decrease of $\sigma_{0.2\%}(T)$ is more pronounced in the low temperature regime. This indicates that the two temperature regimes correspond to two different deformation mechanisms at low and high temperatures.

Hansen [45] has compared the effect of direct strengthening (load transfer) and precipitation hardening on the evolution of the flow stress. Fig. 2 of [45] shows the evolution of $\sigma_{0.2\%}$ as a function of temperature for an Al-Cu-Mg-Mn alloy (called hereafter 2124 Al alloy), where precipitation takes place, and an Al/Al_2O_3 composite reinforced by load transfer. The 2124 Al alloy shows a strong $\sigma_{0.2\%}$ dependence with temperature. Two temperature regimes are separated by a sharp drop of $\sigma_{0.2\%}$ attributed to microstructural evolutions in the Al matrix (coarsening and/or dissolution of precipitates). The temperature dependence of $\sigma_{0.2\%}$ for Al/Al_2O_3 composite shows a more monotonic behaviour attributed to the stability of the Al_2O_3 reinforcement precipitates over the investigated temperature range. At low temperatures ($T \leq 473$ K), the 2124 Al alloy exhibits a $\sigma_{0.2\%}$ higher than that of the Al/Al_2O_3 composite, whereas at higher temperatures ($T > 473$ K), the opposite is observed. In the case of the Al/ω-Al-Cu-Fe composite, the $\sigma_{0.2\%}$ temperature dependence (Fig. 3b) suggests that direct and indirect strengthening contributions are added. For $T \leq 423$ K, the $\sigma_{0.2\%}$ temperature dependence is mainly controlled by the indirect strengthening, whereas for $T \geq 523$ K, load transfer is predominant. The drop of $\sigma_{0.2\%}$ in the temperature range 473 K–523 K cannot be ascribed to load transfer between Al matrix to ω-Al-Cu-Fe particles, which by essence is not thermally activated, but is due to microstructural modifications of the Al matrix during the test. At 573 K, precipitate coarsening takes place during the preliminary heating step prior to deformation. According to Da Costa Teixeira et al. [44], at 473 K, 4 h are necessary to initiate coarsening effects. As a consequence, for $T \leq 473$ K, no coarsening occurs before compression test.

Two sources of indirect strengthening are identified in the Al matrix: the Al(Cu) solid solution strengthening and the structural strengthening due to the θ′-Al_2Cu precipitates. The flow stress of a solid solution strengthened alloy presents two temperature regimes: a first regime at low temperature, where the flow stress is thermally activated and decreases with increasing temperature, followed by a second regime above a temperature T_p, where the flow stress becomes athermal and exhibits a plateau [46-47]. Podkuyko and Pustovalov [48] have experimentally determined that, for Al alloys, T_p is about 200 K. Thus, in our case in the temperature range 273 K–823 K, Al(Cu) solid solution hardening can be reasonably considered as not thermally activated and cannot account for the decrease of $\sigma_{0.2\%}(T)$ for $T < 573$ K.

Precipitation hardening of aluminum alloys can involve either precipitate shearing, for coherent precipitates, or precipitate by-passing by the dislocations. Guyot [49] has shown that, when the two mechanisms are possible, the operating mechanism depends on the precipitate radius. Our TEM observations performed on the composite deformed at room temperature have shown the presence of dislocation loops around the θ′-Al_2Cu precipitates and also smaller loops in the Al matrix. These observations suggest that these semi-coherent precipitates are shear-resistant and that dislocation movement is controlled by a bypass mechanism. Such observations are consistent with Da Costa et al. results [44]. Loops around precipitates are characteristic of the by-pass Orowan mechanism. However, the Orowan mechanism is not thermally activated and depends on temperature only by the elastic coefficients. Several different thermally activated by-passing mechanisms can also produce similar loops, around the precipitates or in their vicinity, such as for instance cross-slip or climb processes [24], which makes very difficult to unambiguously identify the involved mechanism from post-mortem observations.

For $T \geq 523$ K, according to Hansen [45], load transfer becomes predominant. For the 2124 Al alloy, the temperature dependence of the $\sigma_{0.2\%}$ stress is also less pronounced than in the low temperature regime due to a change in the deformation mechanism. Both contributions explain the evolution of $\sigma_{0.2\%}(T)$ observed for the Al/ω-Al-Cu-Fe composites. At 723 K, the presence of a nearly constant curing stage suggests that dislocation multiplication must be compensated by dislocation annihilation involving a restoration process, as it is generally observed in Al alloys. TEM observations do not give evidence of dislocation loops, thus indicating a change in the by-pass mechanisms at high temperature.

4.2. Comparison Between SPS and HIP Composites

A previous study has reported the microstructures and the mechanical behaviours of Al/40 vol%ω-Al-Cu-Fe composite synthesized by hot isostatic pressing (HIP) of i-AlCuFe and commercial Al powders [15,17,50]. Like for the SPS composites, chemical EDS analyses revealed Cu diffusion into the Al matrix, with in this case a maximum Cu content of nearly 2 at.% [50]. TEM observations into the Al matrix of the HIP composites reveal the presence of ω-Al-Cu-Fe nanoparticles aligned along specific crystallographic directions of the Al grains [15]. Laplanche [50] also reported the presence of some large θ-Al_2Cu incoherent precipitates and a few semi-coherent θ′-Al_2Cu precipitates (Fig. 7).

For the SPS composites, the microstructure is characterized by the presence of θ′-Al_2Cu semi-coherent precipitates homogeneously distributed in the Al matrix (see Fig. 4). The difference of the crystallographic structure of the Al_2Cu precipitates in the Al matrix (θ′-Al_2Cu in SPS composites and θ-Al_2Cu in HIP composites) is believed to result from the different dwelling time applied for the synthesis of the composites: 2 min for the SPS composites and 120 min for the HIP composites. Depending on the dwelling time, different stages in the precipitation sequence of Al-Cu alloys are reached:

$$\begin{aligned}\text{Guinier} - \text{Preston zones} &\rightarrow \theta'' - Al_2Cu \text{ (coherent)}\\ &\rightarrow \theta' - Al_2Cu \text{ (semi} - \text{coherent)}\\ &\rightarrow \theta - Al_2Cu \text{ (incoherent).}\end{aligned}$$

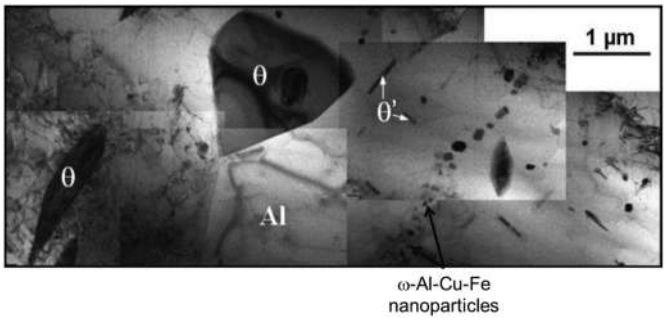

Fig. 7. Bright field TEM images for as-produced Al/ω-Al-Cu-Fe HIP composite, highlighting the presence of θ-Al_2Cu precipitates and ω-Al-Cu-Fe nanoparticles in the Al matrix.

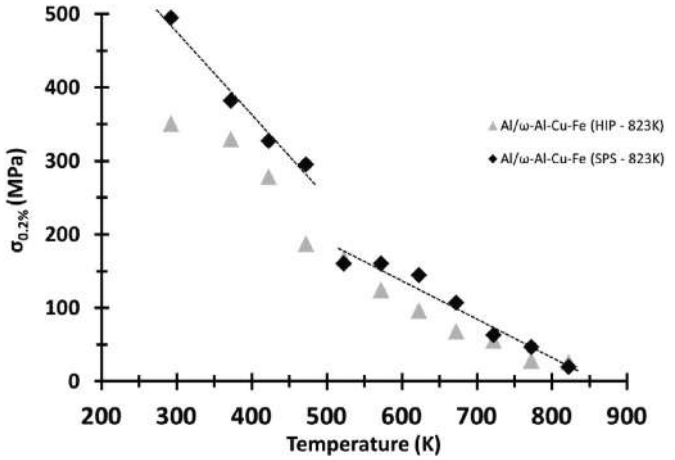

Fig. 8. $\sigma_{0,2\%}$ stress as a function of temperature for Al and Al/ω-Al-Cu-Fe composites synthesized by SPS and HIP techniques.

The temperature dependence of the $\sigma_{0.2\%}$ stress of the HIP composite and the SPS composite are given in Fig. 8 for comparison. For the two types of composite, $\sigma_{0.2\%}(T)$ continuously decreases with increasing temperature; the dependence being very similar. Two temperature regimes are also clearly identified for the HIP composite with a transition temperature in the range 423 K–473 K.

In the low temperature regime, the $\sigma_{0.2\%}$ stress of the SPS composites is higher than that of the HIP composites. In this temperature regime, the stress difference in $\sigma_{0.2\%}$ between SPS and HIP composites is ascribed to the different reinforcement phases present in the Al matrix. On the one hand, it is well known that, for the Al-Cu alloys, the peak of hardening is related to the θ′-Al_2Cu precipitation, while, on the other hand, El Kabir et al. [15] attribute the indirect strengthening in the HIP composites to the presence of ω-Al-Cu-Fe nanoparticles. Our results indicate that θ′-Al_2Cu precipitates homogeneously distributed in the Al matrix lead to a more efficient strengthening.

In the high temperature regime, the temperature dependence of $\sigma_{0.2\%}$ is comparable for the two composites. At such temperatures and according to the previous hypothesis, load transfer is the main strengthening effect. Therefore, whatever the processing route used to produce the composites, the load transfer effect is similar for the two Al/ω-Al-Cu-Fe composites since the volume fraction of reinforcement particles is the same in both cases (40 vol% ω-Al-Cu-Fe) [15].

5. Conclusions

Al-based MMCs reinforced by ω-Al-Cu-Fe particles were produced by SPS from total reaction between Al and i-Al-Cu-Fe powders. Compression tests at constant strain rate were performed over the temperature range 293 K–823 K. The composite microstructure was studied by SEM observations coupled with post-mortem and *in-situ* heating TEM observations of the Al matrix. The main results and interpretations can be summarized as follows.

The phase transformation from the initial icosahedral phase to the ω crystalline phase leads to diffusion of Cu into the Al matrix and to precipitation of θ′-Al_2Cu. Because ω-Al-Cu-Fe particles are, like QC-Al-Cu-Fe particles, hard particles, plastic deformation of the Al/ω-Al-Cu-Fe composite is ascribed at all temperatures to the Al matrix only. The continuous decrease of the $\sigma_{0,2\%}$ proof stress with increasing temperature highlights the role of thermal activation in the deformation mechanisms of the composite in the investigated temperature range. A transition temperature is observed in the temperature range 473 K–523 K. Considering that load transfer is not thermally activated, the drop of $\sigma_{0,2\%}$ values is attributed to microstructural changes in the Al matrix during the deformation test, in particular to the coarsening of the Al_2Cu precipitates. It is worth noting that this coarsening is strongly temperature and time dependent. This underlines the importance of the experimental procedures for such a type of composite which must be designed to deform samples having stable microstructures with respect to the deformation temperature. The temperature dependence of $\sigma_{0,2\%}$ was compared to that of Al/ω-Al-Cu-Fe composite obtained by a HIP process. Similar characteristics are observed, that are a continuous decrease of $\sigma_{0,2\%}$ with increasing temperatures and the existence of two well-defined temperature regimes. In the low temperature regime, the $\sigma_{0.2\%}$ stress of the SPS composites is higher than that of the HIP composites. In this temperature regime, the stress difference in $\sigma_{0.2\%}$ is mainly ascribed to the different reinforcement phases present in the Al matrix grains, *i.e.* Al_2Cu precipitates for the SPS composite *versus* ω-Al-Cu-Fe nanoparticles for the HIP composite. In the high temperature regime, the temperature dependence of $\sigma_{0.2\%}$ is comparable for the two composites. This indicates that at such temperatures, whatever the processing route used to produce the composites, load transfer is the main strengthening mechanism which is similar for the two Al/ω-Al-Cu-Fe composites.

Acknowledgement

This work was supported by the “Agence Nationale de la Recherche” as part of FutureAlCo project (ANR 13-BS09-005-01). G. Laplanche (University of Bochum, Germany) is kindly acknowledged for providing i-Al-Cu-Fe quasicrystalline phase ingots. A. Joseph thanks French Government program “Investissements d'Avenir” (LABEX INTERACTIF, ANR-11-LABX-0017-01) for a one-year post-doctoral position.

Data Availability

The authors do not have permission to share data.

References

[1] T.W. Clyne, P.J. Withers, An Introduction to Metal Matrix Composites, Cambridge University Press, 1995.
[2] D.J. Lloyd, Particle reinforced aluminium and magnesium matrix composites, Int. Mater. Rev. 39 (1994) 1–23, https://doi.org/10.1179/imr.1994.39.1.1.
[3] A. Evans, C. SanMarchi, A. Mortensen, Metal Matrix Composites in Industry: An Introduction and a Survey, Kluwer Academic, 2003.
[4] N. Chawla, K.K. Chawla, Metal Matrix Composites, Springer, 2006.
[5] D.B. Miracle, Metal matrix composites – from science to technological significance, Compos. Sci. Technol. 65 (2005) 2526–2540, https://doi.org/10.1016/j.compscitech.2005.05.027.
[6] R.M. Aikin, The mechanical properties of in-situ composites, JOM 49 (1997) 35, https://doi.org/10.1007/BF02914400.
[7] M. Singh, D. Lewis, In Situ Composites: Science and Technology, The Minerals, Metals & Materials Society, Warrendale, Pa, 1994.
[8] S.L. Pramod, S.R. Bakshi, B.S. Murty, Aluminum-based cast in situ composites: a review, J. Mater. Eng. Perform. 24 (2015) 2185–2207, https://doi.org/10.1007/s11665-015-1424-2.
[9] A.P. Tsai, K. Aoki, A. Inoue, T. Masumoto, Synthesis of stable quasicrystalline particle-dispersed Al base composite alloys, J. Mater. Res. 8 (1993) 5–7, https://doi.org/10.1557/JMR.1993.0005.
[10] F. Tang, I.E. Anderson, S.B. Biner, Microstructures and mechanical properties of pure Al matrix composites reinforced by Al-Cu-Fe alloy particles, Mater. Sci. Eng. A 363 (2003) 20–29, https://doi.org/10.1016/S0921-5093(03)00433-7.
[11] F. Tang, The Microstructure-processing-property Relationships in an Al Matrix Composite System Reinforced by Al-Cu-Fe Alloy Particles (Retrosp. Theses Diss.),, 2004. http://lib.dr.iastate.edu/rtd/818.
[12] F. Tang, T. Gnäupel-Herold, H. Prask, I.E. Anderson, Residual stresses and stress partitioning measurements by neutron diffraction in Al/Al–Cu–Fe composites, Mater. Sci. Eng. A 399 (2005) 99–106, https://doi.org/10.1016/j.msea.2005.02.027.
[13] F. Schurack, J. Eckert, L. Schultz, Synthesis and mechanical properties of mechanically alloyed Al-Cu-Fe quasicrystalline composites, Philos. Mag. 83 (2003) 1287–1305, https://doi.org/10.1080/1478643031000076613.
[14] S.M. Lee, J.H. Jung, E. Fleury, W.T. Kim, D.H. Kim, Metal matrix composites reinforced by gas-atomised Al-Cu-Fe powders, Mater. Sci. Eng. A 294–296 (2000) 99–103, https://doi.org/10.1016/S0921-5093(00)01223-5.
[15] T. El Kabir, A. Joulain, V. Gauthier, S. Dubois, J. Bonneville, D. Bertheau, Hot isostatic pressing synthesis and mechanical properties of Al/Al–Cu–Fe composite materials, J. Mater. Res. 23 (2008) 904–910, https://doi.org/10.1557/jmr.2008.0111.
[16] G. Laplanche, A. Joulain, J. Bonneville, V. Gauthier-Brunet, S. Dubois, Synthesis

and brittle-to-ductile transition of the ω-$Al_{0.7}Cu_{0.2}Fe_{0.1}$ tetragonal phase, Mater. Sci. Eng. A 527 (2010) 4515–4518, https://doi.org/10.1016/j.msea.2010.02.049.
[17] G. Laplanche, A. Joulain, J. Bonneville, V. Gauthier-Brunet, S. Dubois, T. El Kabir, Microstructural and mechanical study of an Al matrix composite reinforced by Al-Cu-Fe icosahedral particles, J. Mater. Res. 25 (2010) 957–965, https://doi.org/10.1557/JMR.2010.0118.
[18] S.D. Kaloshkin, V.V. Tcherdyntsev, A.I. Laptev, A.A. Stepashkin, E.A. Afonina, A.L. Pomadchik, V.I. Bugakov, Structure and mechanical properties of mechanically alloyed Al/Al-Cu-Fe composites, J. Mater. Sci. 39 (2004) 5399–5402, https://doi.org/10.1023/B:JMSC.0000039253.28721.3f.
[19] S. Kenzari, P. Weisbecker, M. Curulla, G. Geandier, V. Fournee, J.M. Dubois, Formation and properties of Al composites reinforced by quasicrystalline AlCuFeB particles, Philos. Mag. 88 (2008) 755–766, https://doi.org/10.1080/14786430801955253.
[20] L. Lityńska-Dobrzyńska, J. Dutkiewicz, K. Stan-Głowińska, W. Wajda, L. Dembinski, C. Langlade, C. Coddet, Characterization of aluminium matrix composites reinforced by Al–Cu–Fe quasicrystalline particles, J. Alloys Compd. 643 (Supplement 1) (2015) S114–S118, https://doi.org/10.1016/j.jallcom.2014.11.125.
[21] L. Lityńska-Dobrzyńska, M. Mitka, A. Góral, K. Stan-Głowińska, J. Dutkiewicz, Microstructure and mechanical properties of aluminium matrix composites reinforced by $Al_{62}Cu_{25.5}Fe_{12.5}$ melt spun ribbon, Mater. Charact. 117 (2016) 127–133, https://doi.org/10.1016/j.matchar.2016.04.025.
[22] W. Wolf, L.C.R. Aliaga, D.N. Travessa, C.R.M. Afonso, C. Bolfarini, C.S. Kiminami, W.J. Botta, Enhancement of mechanical properties of aluminum and 2124 aluminum alloy by the addition of quasicrystalline phases, Mater. Res. 19 (2016) 74–79, https://doi.org/10.1590/1980-5373-mr-2016-0088.
[23] F. Ali, S. Scudino, G. Liu, V.C. Srivastava, N.K. Mukhopadhyay, M. Samadi Khoshkhoo, K.G. Prashanth, V. Uhlenwinkel, M. Calin, J. Eckert, Modeling the strengthening effect of Al–Cu–Fe quasicrystalline particles in Al-based metal matrix composites, J. Alloys Compd. 536 (Supplement 1) (2012) S130–S133, https://doi.org/10.1016/j.jallcom.2011.12.022.
[24] F. Ali, S. Scudino, M.S. Anwar, R.N. Shahid, V.C. Srivastava, V. Uhlenwinkel, M. Stoica, G. Vaughan, J. Eckert, Al-based metal matrix composites reinforced with Al–Cu–Fe quasicrystalline particles: strengthening by interfacial reaction, J. Alloys Compd. 607 (2014) 274–279, https://doi.org/10.1016/j.jallcom.2014.04.086.
[25] F. Schurack, J. Eckert, L. Schultz, Synthesis and mechanical properties of cast quasicrystal-reinforced Al-alloys, Acta Mater. 49 (2001) 1351–1361, https://doi.org/10.1016/S1359-6454(01)00045-3.
[26] T.J. Watson, M.A. Gordillo, I. Cernatescu, M. Aindow, Structure and mechanical properties in a powder-processed icosahedral-phase-strengthened aluminum alloy, Scr. Mater. 123 (2016) 51–54, https://doi.org/10.1016/j.scriptamat.2016.05.037.
[27] N. Kang, Y. Fu, P. Coddet, B. Guelorget, H. Liao, C. Coddet, On the microstructure, hardness and wear behavior of Al-Fe-Cr quasicrystal reinforced Al matrix composite prepared by selective laser melting, Mater. Des. 132 (2017) 105–111, https://doi.org/10.1016/j.matdes.2017.06.060.
[28] J. Bonneville, D. Caillard, P. Guyot, Dislocations and plasticity of icosahedral quasicrystals, in: J.P. Hirth (Ed.), Dislocations Solids, North-Holland, Elsevier, 2008, pp. 251–331.
[29] M. Texier, A. Proult, J. Bonneville, On the plasticity of Al–Cu–Fe quasicrystals, Mater. Sci. Eng. A 400–401 (2005) 315–319, https://doi.org/10.1016/j.msea.2005.02.089.
[30] M. Texier, J. Bonneville, A. Proult, J. Rabier, N. Baluc, P. Guyot, On the yield point of icosahedral AlCuFe quasicrystals, Scr. Mater. 49 (2003) 41–46, https://doi.org/10.1016/S1359-6462(03)00171-4.
[31] G. Laplanche, J. Bonneville, A. Joulain, V. Gauthier-Brunet, S. Dubois, Mechanical properties of Al–Cu–Fe quasicrystalline and crystalline phases: an analogy, Intermetallics 50 (2014) 54–58, https://doi.org/10.1016/j.intermet.2014.02.004.
[32] E. Giacometti, N. Baluc, J. Bonneville, Activation parameters of plastic flow in icosahedral Al-Cu-Fe, Philos. Mag. Lett. 79 (1999) 1–7, https://doi.org/10.1080/095008399177598.
[33] E. Giacometti, J. Fikar, N. Baluc, J. Bonneville, Mechanical behaviour versus structure of $Al_{63.6}Cu_{24.0}Fe_{12.4}$, Philos. Mag. Lett. 82 (2002) 183–189, https://doi.org/10.1080/09500830110117798.
[34] A. Joseph, V. Gauthier-Brunet, J.P. Monchoux, A. Joulain, F. Brisset, C. Tromas, J. Douin, F. Pettinari, J. Bonneville, S. Dubois, Formation processes of the ω-Al70Cu20Fe10 phase synthesized by SPS technique, J. Alloys Compd. 699 (2017) 1157–1165, https://doi.org/10.1016/j.jallcom.2016.12.221.
[35] B. Viguier, A. Mortensen, Heating of TEM specimens during ion milling, Ultramicroscopy 87 (2001) 123–133, https://doi.org/10.1016/S0304-3991(00)00095-4.
[36] J. Bonneville, N. Baluc, Deformation regimes in the intermetallic alloys, Ni3Al, in: O. Izumi (Ed.), Proc Int Symp Intermet. Compd. Struct. Mech. Prop, The Japan Institut of Metals, 1991, pp. 323–330.
[37] X. Zhang, T. Hu, J.F. Rufner, T.B. LaGrange, G.H. Campbell, E.J. Lavernia, J.M. Schoenung, K. van Benthem, Metal/ceramic interface structures and segregation behavior in aluminum-based composites, Acta Mater. 95 (2015) 254–263, https://doi.org/10.1016/j.actamat.2015.05.021.
[38] M.V. Lancker, Metallurgy of Aluminium Alloys, Chapman & Hall, 1967.
[39] G. Laplanche, J. Bonneville, A. Joulain, V. Gauthier-Brunet, S. Dubois, Plasticity of the ω-Al_7Cu_2Fe phase, J. Alloys Compd. 665 (2016) 144–151, https://doi.org/10.1016/j.jallcom.2015.12.161.
[40] J.D. Boyd, R.B. Nicholson, The coarsening behaviour of θ″ and θ′ precipitates in two Al-Cu alloys, Acta Metall. 19 (1971) 1379–1391, https://doi.org/10.1016/0001-6160(71)90076-9.
[41] R. Sankaran, C. Laird, Kinetics of growth of platelike precipitates, Acta Metall. 22 (1974) 957–969, https://doi.org/10.1016/0001-6160(74)90021-2.
[42] P. Merle, F. Fouquet, Coarsening of θ' plates in Al-Cu alloys—I. experimental determination of mechanisms, Acta Metall. 29 (1981) 1919–1927, https://doi.org/10.1016/0001-6160(81)90029-8.
[43] P. Merle, J. Merlin, Coarsening of θ' plates in Al-Cu alloys—II. Influence of ledge mechanism, Acta Metall. 29 (1981) 1929–1938, https://doi.org/10.1016/0001-6160(81)90030-4.
[44] J. da Costa Teixeira, D.G. Cram, L. Bourgeois, T.J. Bastow, A.J. Hill, C.R. Hutchinson, On the strengthening response of aluminum alloys containing shear-resistant plate-shaped precipitates, Acta Mater. 56 (2008) 6109–6122, https://doi.org/10.1016/j.actamat.2008.08.023.
[45] N. Hansen, Dispersion-strengthened Aluminium Products (Thesis, 157 p.), Forskningscenter Risoe. Risoe-R; No. 223, Denmark, 1971.
[46] M.Z. Butt, P. Feltham, Solid-solution hardening, Acta Metall. 26 (1978) 167–173, https://doi.org/10.1016/0001-6160(78)90213-4.
[47] M.Z. Butt, P. Feltham, Solid-solution hardening, J. Mater. Sci. 28 (1993) 2557–2576, https://doi.org/10.1007/BF00356192.
[48] V.P. Podkuyko, V.V. Pustovalov, Peculiar mechanical properties of aluminium-magnesium, aluminium-copper and aluminium-zinc alloys at low temperatures, Cryogenics 18 (1978) 589–595, https://doi.org/10.1016/0011-2275(78)90019-X.
[49] P. Guyot, Hardening by ordered coherent precipitates related to the statistical theory, Philos. Mag. 24 (1971) 987–993, https://doi.org/10.1080/14786437108217063.
[50] G. Laplanche, Guillaume Laplanche - Synthèse et caractérisation de la phase ω-Al7Cu2Fe et de composites Al/Al-Cu-Fe, Poitiers (2011).